Journal of Aerosol Science 149 (2020) 105605

Contents lists available at ScienceDirect

Journal of Aerosol Science

journal homepage: http://www.elsevier.com/locate/jaerosci

Estimation of the deposition of ultrafine 3D printing particles in human tracheobronchial airways

Wei-Chung Su [a,*], Yi Chen [a], Jinxiang Xi [b]

[a] Department of Epidemiology, Human Genetics and Environmental Sciences, School of Public Health, University of Texas Health Science Center at Houston, Houston, TX, USA

[b] Department of Biomedical Engineering, Francis College of Engineering, University of Massachusetts, Lowell, MA, USA

ARTICLE INFO

Keywords:
Ultrafine particles
3D printer
Respiratory deposition
Bifurcation generation

ABSTRACT

3D printers have been widely used as a tool for prototype manufacturing in industries, schools, and homes. During operation, 3D printers emit ultrafine particles that could be inhaled by the user and induce adverse health effects. Thus, exposure to ultrafine 3D-printing generated particles has drawn the attention of occupational and environmental health researchers. In this study, a recently developed Mobile Aerosol Lung Deposition Apparatus (MALDA) was applied to investigate the respiratory deposition of ultrafine 3D printing particles. The MALDA consists of a set of representative human airway replicas from mouth, throat, trachea, down to the bronchiolar airways of the 11th bifurcation generation. A series of respiratory deposition experiments were carried out in the laboratory using the MALDA and a desktop 3D printer to estimate the deposition of ultrafine 3D printing particles in individual generations of the lung. Results showed that the cumulative deposition from the 1st to 11th bifurcation generations was found to be 1%–13% depending on the particle size, which was slightly less than the respiratory deposition predicted from the conventional deposition curve.

1. Introduction

To date, due to the features of easy-to-use and low-cost, 3D printers have been widely used as a tool for prototype manufacturing, education, and hobbies in industries, schools, and homes (Campbell et al., 2011). Among different types of 3D printing technologies, Fused Deposition Modeling (FDM) is the most commonly used 3D printing technique (Zukas & Zukas, 2015). While operating, the nozzle of the FDM 3D printer heats up the filament (printing material) to a semi-liquid state, then extrudes and deposits the material on a supporting object layer-by-layer to build the designed 3D project (Lipson & Kurman, 2013). During the filament-heating and printing processes, vapors of the printing materials and additives are emitted due to evaporation or thermal decomposition caused by high temperature (Deng et al., 2016; Potter et al., 2019; Wojtyła et al., 2017). Some of the chemical vapor might condense/nucleate into small particles after encountering relatively cooler air away from the printer nozzle (Gu et al., 2019; Stabile et al., 2017). Based on this particle formation process, aerosols generated from the FDM 3D printer typically are ultrafine particles with particle diameters less than 100 nm in general (Vance et al., 2017). Ultrafine particles generated by the FDM 3D printers were commonly singular and spherical in shape (Zhang et al., 2017). However, the particle emission rates could vary depending on the heating temperature and the

* Corresponding author. Department of Epidemiology, Human Genetics & Environmental Sciences, University of Texas, Health Science Center at Houston, 1200 Pressler St. Houston, TX, 77030, USA.

E-mail address: Wei-Chung.Su@uth.tmc.edu (W.-C. Su).

https://doi.org/10.1016/j.jaerosci.2020.105605
Received 11 February 2020; Received in revised form 21 May 2020; Accepted 28 May 2020
Available online 20 June 2020
0021-8502/

type of filament materials. For instance, the acrylonitrile-butadiene-styrene (ABS) filament generates an overall higher concentration of ultrafine particles than the polylactic acid (PLA) filaments do (Azimi et al., 2016). Because of their nano-scaled sizes and low terminal setting velocities, ultrafine particles can suspend in the air for a considerable period of time (Hinds, 1999). Therefore, ultrafine 3D printing particles would inevitably be inhaled by the 3D printer users. The inhalation and deposition of such particles in the human respiratory tract could lead to various adverse health effects such as asthma (House et al., 2017) and respiratory inflammation (Chan et al., 2017). The exposure to ultrafine 3D printing particles, therefore, has gradually become an emerging occupational and environmental health concern (Stephens et al., 2013). Besides, it is known that the inhalation of ultrafine particles could induce stronger responses than larger particles of the same chemical composition per given mass, and systemic translocations could take place after particle deposition (Kreyling et al., 2006; Oberdörster, 2001). Therefore, studying the respiratory deposition of ultrafine 3D printing particles is essential from the viewpoint of public health. Obtaining reliable respiratory deposition data can assist the estimation of the inhalation dose, which can greatly benefit the 3D printer related exposure assessments and health risk analyses.

However, as of today, no respiratory deposition experiments have been reported for ultrafine 3D printing particles. This might be attributed to the limitations of the traditional experimental methods used for aerosol respiratory deposition studies. One limitation was that the deposited particles needed to be counted or recovered from the human airway replica in order to estimate the deposition fraction (Cheng et al., 1999; Su & Cheng, 2009). However, traditional methodologies were time-consuming and labor-intensive, which greatly hampered their application. The other limitation of the traditional experimental methods was associated with the availability of anatomically accurate lower airway replicas for respiratory deposition experiments. Because of the technical challenges in developing realistic lung models, airway replicas used in previous studies possessed only a partial portion of the lung down to the 4th to 7th bifurcation generation (Smith et al., 2001; Su et al., 2016; Zhou & Cheng, 2005). One exception was Phalen et al. (1997) who developed a cadaver-based lung replica cast consisting of 9th to 11th bifurcation generations. However, the upper respiratory tract was not included in their study. Given that merely a few bifurcation generations were retained in the replica of the tracheobronchial (TB) airways, useful information provided by the deposition experiments using such airway replicas was limited. Moreover, it is shown that the deposition efficiencies of inhaled ultrafine particles increase in more distal airways from the 4th bifurcation generation (Smith et al., 2001). Therefore, a novel experimental method that incorporates a human lower airway replica is needed to investigate the ultrafine particle deposition in TB airways.

With the above in mind, an innovative experimental approach based on the Mobile Aerosol Lung Deposition Apparatus (MALDA) was recently developed in our laboratory (Su et al., 2019a, 2019b). The purpose of the development of MALDA was to facilitate occupational and environmental on-site ultrafine particle respiratory deposition studies especially for those ultrafine particles with non-spherical shapes (e.g. elongated particles or agglomerates). Due to the effect of the irregular particle shape on the particle behavior in the air, the respiratory deposition fraction of irregular ultrafine particles might not be correctly predicted by the convention respiratory deposition curves because these convention curves were established mainly based on singular, spherical particles. In this study, significant upgrades were made to the MALDA including making a new, delicate TB airway replica down to the 11th bifurcation generation. A series of respiratory deposition experiments were conducted using the upgraded MALDA to estimate the respiratory deposition of ultrafine 3D printing particles in individual TB generations under inspiratory flow rate. Data obtained showed new experimental data of ultrafine particle respiratory deposition in the human TB airways down to the 11th bifurcation generation.

2. Material and methods

2.1. Generation of ultrafine 3D printing particles

In this study, ultrafine 3D printing particles used in the deposition experiments were generated by a desktop 3D printer (LulzBot Mini2, Aleph Objects, Inc., Loveland, CO) using 2.88 mm ABS filament in purple color (Keene Village Plastics, Barberton, OH). The 3D printer was placed inside a stainless steel chamber with a dimension of 61 cm × 61 cm × 61 cm. The 3D printer was operated with manufacturer default printing parameters and programmed to print a short vertical cylinder 10 mm in diameter and 12 mm in height (printing temperature: 245 °C). The complete procedure to print the short cylinder was about 20 min.

2.2. Mobile aerosol lung deposition apparatus (MALDA)

The MALDA used in this deposition experiment consisted of two major systems: the simplified human airway system and the ultrafine particle measurement system. It is the synergy of these two systems that makes an efficient and systematic aerosol respiratory deposition measurement feasible with using MALDA. The simplified human airway system incorporates a set of human airway replicas from the mouth, oropharynx, larynx, trachea, down to a certain bifurcation generation in the TB airways. In our previous study, 10 human airway replicas were made for the MALDA (R0 to R9). The R0 indicates that the airway replica extends from the oral cavity to the trachea only (0 bifurcation generation). The R9 indicates that the airway replica extends from the oral cavity to the 9th bifurcation generation, etc. To upgrade the function of the MALDA, two additional human TB airway replicas were made (R10 and R11). The R11 contains small airways down to the 11th bifurcation generation with 3311 airway branches and the smallest branch diameter is 1.15 mm. The 3D digital files of human TB airway replicas were developed using the software Lung4Cer published by Kitaoka et al. (2013). The inner diameter of the trachea (d_0) was 18 mm. The inner diameters of the two daughter branches (d_1 and d_2) were calculated based on the minimum energy loss principle: $d_1 = d_0 r^{1/2.8}$ and $d_2 = d_0 (1\text{-}r)^{1/2.8}$, where r is the flow partition between the two daughter branches (Kitaoka et al., 1999). The length-to-diameter ratio was 2.8, and the branching angles of the two daughter branches (θ_1 and θ_2) were determined by:

$$\cos\theta_1 = \left[1 + r^{4/3} - (1-r)^{4/3}\right] / 2r^{2/3}; \cos\theta_2 = \left[1 + (1-r)^{4/3} - r^{4/3}\right] / 2(1-r)^{2/3} \quad (1)$$

Fig. 1 shows the computer model and the physical model of the TB airways down to the 11th bifurcation generation. The inclusion of a respiratory tract replica down to the 11th generation is a substantial function enhancement for the MALDA compared to its previous version. In this study, TB airway replicas with lower bifurcation generations were made by a high-resolution 3D printer, PolyJet J750 (Stratasys Ltd., Valencia, California, USA), which provides printing layer thickness as fine as 0.014 mm. Thus, ridges resulting from the 3D printing in the inner surface of the TB airway replicas are considered minimal. More information regarding the development and making of TB airway replicas can be found in our previous publication (Su et al., 2019). To use airway replicas for respiratory deposition experiments, the inner surface of the airway replica was coated with silicon oil to mimic the wet inner-surface nature of the human respiratory tract.

The ultrafine particle measurement system comprises two Scanning Mobility Particle Spectrometers (SMPS + C, GRIMM Aerosol Technology, Germany), which are capable of measuring the particle size distribution (number concentration) from 5 nm to 350 nm with 44 size channels. The two particle sizers work to record the size distribution of the ultrafine 3D printing particles before and after particles passing through the simplified human airway system. The difference of the particle size distribution found between the inlet and outlet of the simplified human airway system will be used to calculate the deposition of ultrafine 3D printing particles in the TB airways. Fig. 2 depicts the schematic diagram and key components of the MALDA. Details of the principles, design, assembly, and function of the MALDA, as well as the making of human airway replicas, can be found in our previous publications.

2.3. Experimental set-up and procedures

Fig. 3 shows the experimental set-up of the respiratory deposition study using MALDA. The ultrafine particles generated by the 3D printer were delivered from the chamber to the MALDA standing aside through a conductive tube. The inspiratory flow rate used in the deposition experiment was 30 L/min for all TB airway replicas employed in this study (MALDA only measured particle depositions during inhalation). The two ultrafine particle sizers (SMPS + C) were connected to two designated sampling probes, which are located at the oral inlet and the Y-shape connector outlet, respectively (Fig. 3). In this way, size-dependent ultrafine particle number concentrations were recorded before (C_{in}) and after (C_{out}) particles passing through the simplified human airway system. If the outlet-to-inlet concentration ratio (C_{out}/C_{in}) shows less than 1.0, it indicates particles deposited in the simplified human airway system. By changing the human airway replicas from R0 to R11, size-dependent particle concentration ratios (C_{out}/C_{in}) can be systematically and efficiently obtained using MALDA to estimate the respiratory deposition of ultrafine 3D printing particles in individual bifurcation generations.

2.4. Estimation of the respiratory deposition for ultrafine 3D printing particles

To estimate particle deposition fractions in individual bifurcation generations in the TB airways, the outlet-to-inlet concentration ratios (C_{out}/C_{in}) measured from two adjacent TB airway replicas (*Ri* and *R(i-1)*) were used for back calculating the deposition fraction in a specific bifurcation generation *Gi*. Eq. (2) presents the method to calculate the deposition fraction (%) based on the measured out-to-inlet concentration ratios.

$$D_{d,Gi}(\%) = \left(1 - \frac{C_{out,d,Ri}}{C_{in,d,Ri}}\right) \times 100 - \left(1 - \frac{C_{out,d,R(i-1)}}{C_{in,d,R(i-1)}}\right) \times 100, \quad \mathrm{i} = 1 \text{ to } 11 \quad (2)$$

where $D_{d,Gi}$ is the deposition fraction (%) of ultrafine 3D printing particles with the diameter of d nm deposited in the ith bifurcation generation, *Gi* (the entire ith bifurcation generation). *Ri* represents the simplified human airway system with airway replicas from the

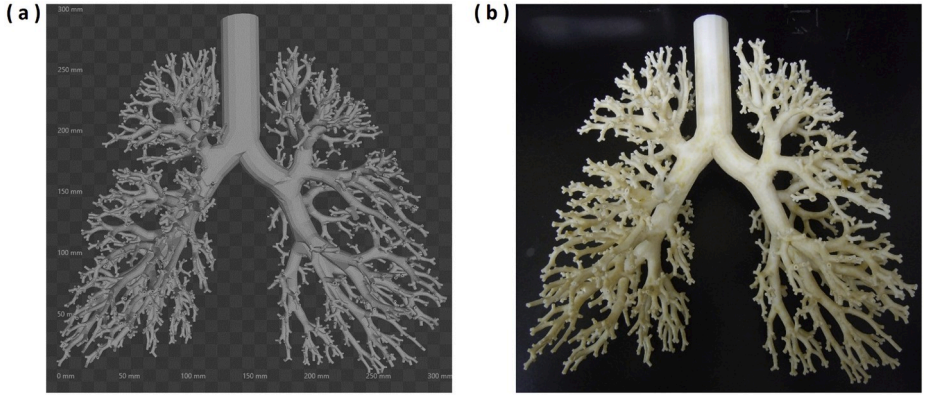

Fig. 1. The human TB airway replica down to the 11th bifurcation generation (a) computer model, and (b) 3D printed physical model.

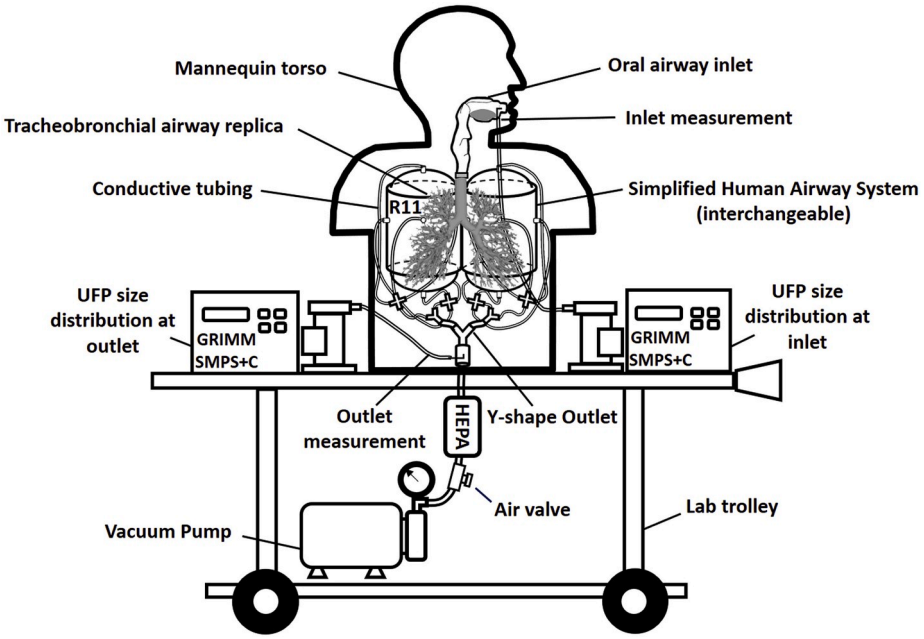

Fig. 2. The schematic diagram of MALDA with the human airway replica R11.

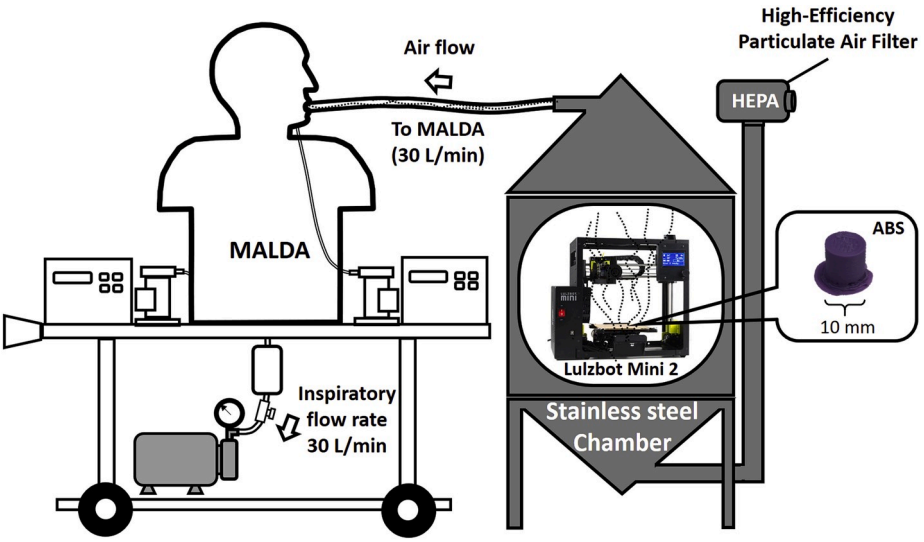

Fig. 3. The experimental set-up of the ultrafine 3D printing particle deposition study using MALDA.

mouth to the *i*th bifurcation generation. $C_{out,d,Ri}$ and $C_{in,d,Ri}$ are the number concentrations of particles with the diameter of d nm measured at the outlet and inlet of the Ri, respectively. $C_{out,d,Ri}/C_{in,d,Ri}$ represents the penetration efficiency, and 1-$C_{out,d,Ri}/C_{in,d,Ri}$ represents the deposition efficiency. Based on Eq. (2), by conducting a series of respiratory deposition experiments systematically using the exchangeable human airway replicas from R0 to R11, a set of size-dependent C_{out}/C_{in} can be acquired. With all the needed C_{out}/C_{in} available, deposition fractions of ultrafine 3D printing particles in each bifurcation generation from G1 to G11 can then be calculated.

In this study, a modified experimental protocol based on the aforementioned principle was designed to complete a set of experiments more efficiently. Instead of testing all airway replicas, only airway replicas in odd numbers (R1, R3, R5, R7, R9, R11, and R0) were implemented in the experiments. In so doing, half of the testing time was saved, and the back-calculated deposition fractions represented particle depositions in two consecutive bifurcation generations instead of one bifurcation generation as in the original design. In this study, deposition experiments for each Ri were repeated at least five times to acquire arithmetic mean and standard deviation. Two particle sizers were frequently cleaned and tested for equivalence. The results of the equivalence tests were recorded and used as the correction factors to correct the measured C_{out}/C_{in} as described in our previous studies (Su et al., 2019). To minimize

the effects of the experimental data variation on the final result, an empirical model based on the measured C_{out}/C_{in} was developed to assist the estimation of particle deposition in individual bifurcation generations. The empirical model was in the format of a function of the airway replica (Ri) and the size of the ultrafine 3D printing particle (d).

$$C_{out}/C_{in} = f_1(Ri) + g(Ri)\ (1 - c\ d^k) \tag{3}$$

where the f and g are functions of Ri, and the c and k are constants that were determined by the experimental data.

In addition, to consider the particle wall-loss within the simplified human airway system, a wall-loss correction equation as a function of Ri and d was also developed.

$$\text{Wall-loss} = \text{L(Ri, d)} \tag{4}$$

The wall-loss correction equation was determined based on the procedures described in our previous research with using the multiple-path particle dosimetry model (MPPD v 3.04) developed by Miller et al. (2016), and a separate set of particle respiratory deposition experiments using laboratory ultrafine particle surrogates. The MPPD model is capable of providing useful information as a reference for particle respiratory deposition in different airway regions. The separate set of deposition experiments were conducted using sodium chloride (NaCl) ultrafine particles. The experimental set-up, procedure, and the MALDA were the same as stated above for the 3D printing study including the inspiratory flow rate (30 L/min). The only difference between these two experiments was the test ultrafine particles. The test NaCl ultrafine particles were generated by a laboratory-grade atomizer (3079A, TSI Inc., Shoreview, MN, USA). The TSI 3079A has been utilized for generating steady and reliable challenge NaCl aerosols for filtration tests (He et al., 2020; Ryi et al., 2007).

With the assist from the empirical model Eq. (3) and the wall-loss correction equation Eq. (4), the deposition fraction of the ultrafine 3D printing particles in the TB airways can be estimated more accurately. The calculation of the respiratory deposition fraction was done first by Eq. (3) + Eq. (4) to take into account the wall-loss in the measured C_{out}/C_{in}, and then the deposition fractions in individual bifurcation generations could be calculated using Eq. (2).

3. Results and discussion

Fig. 4 expresses the size distribution of the particles generated by the 3D printer in the chamber. Fig. 5 shows the TEM (Transmission electron microscopy) morphology analysis of the particles collected during deposition experiments. Data shown in Figs. 4 and 5 were obtained from the time frame of 17–20 min during the 3D printing process. This time frame was also the time frame of carrying out deposition experiments. The choice of this time frame considered the consistency in the particle size distribution, the particle concentration, as well as the temperature inside the chamber. As can be seen, particles emitted from the 3D printer were ultrafine particles with diameters generally being less than 100 nm and the peak of the diameter being around 60 nm–80 nm. From Fig. 5, the morphology of the ultrafine 3D printing particle was shown to be singular spheres.

Fig. 6 shows the measured outlet-to-inlet concentration ratios (C_{out}/C_{in}) plotted against the particle diameter. The C_{out}/C_{in} are lined up by the human airway replicas from R0 to R11 in odd numbers. Data presented are the results after the correction factor adjustment. The correction factor was obtained from the equivalence tests mentioned above. It shows in Fig. 6 that the C_{out}/C_{in} decreased as the particle diameter decreased, which indicates that the dominant deposition mechanism for ultrafine 3D printing particles in the human airways is diffusion (smaller C_{out}/C_{in} implies more airway deposition). Moreover, C_{out}/C_{in} shifted downward progressively from R0 to R11 indicating the effect of the complicated airway structure on the particle deposition in the TB airways.

Based on the experimental data acquired, an empirical model of C_{out}/C_{in} was proposed:

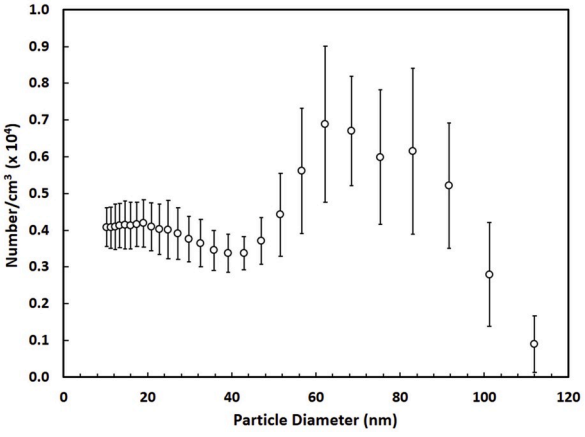

Fig. 4. The size distribution of ultrafine 3D printing particles during the 17–20 min time frame of a 20-min 3D printing project (Error bars represent the standard deviation.).

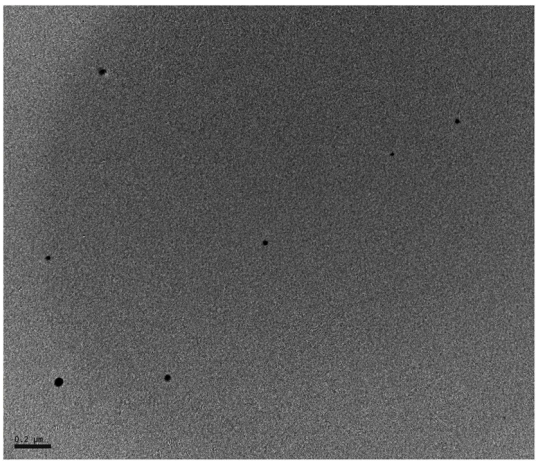

Fig. 5. TEM images of the morphology of ultrafine 3D printing particles (The reference bar represents 0.2 μm).

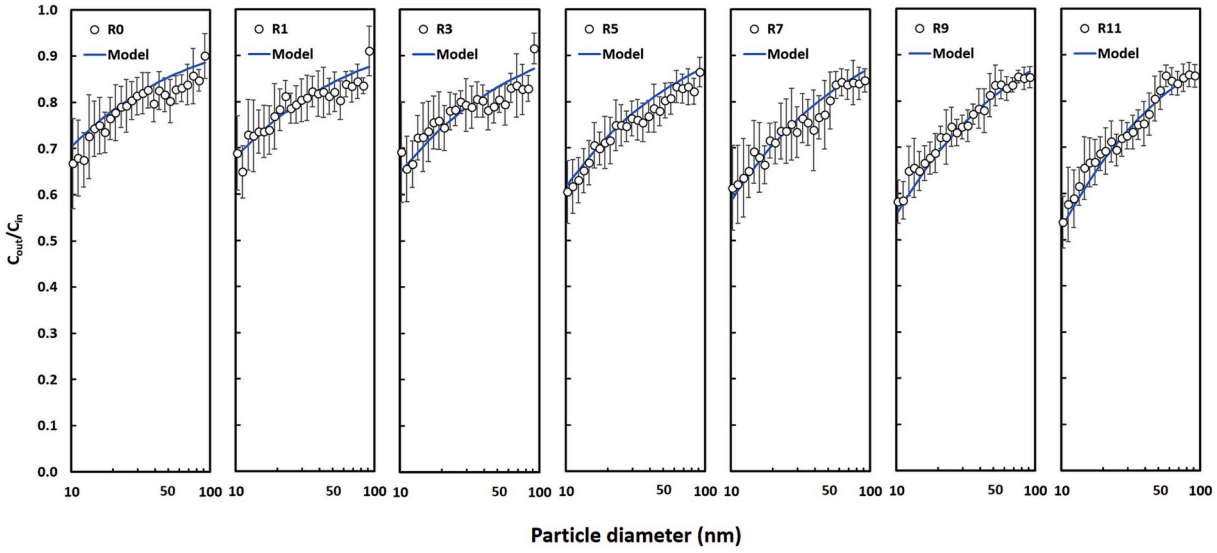

Fig. 6. The experimental data and empirical model data of the outlet-to-inlet concentration ratio (C_{out}/C_{in}) as a function of the particle diameter of the ultrafine 3D printing particles (data presented are the results after the correction factor adjustment, and error bars represent the standard deviation.).

$$\frac{C_{out,d,R}}{C_{in,d,R}} = \left(0.89 - 0.01R^{0.3}\right) + (0.09 + 0.007\mathrm{R})\left(1 - 9.5d^{-0.49}\right) \tag{5}$$

where d is the particle diameter (from 10 to 100 nm), and R is the lowest bifurcation generation used in the airway replica (from 0 to 11). Data calculated by Eq. (5) were plotted together with the experimental data in Fig. 6 for comparison. As can be seen, the proposed empirical model agreed quite well with the experimental data. The coefficient of determination of the empirical model (R^2) reached 0.93 (Fig. 7). This result demonstrates that the empirical model can ideally catch the trend and pattern of the experimental data. Therefore, it is appropriate to use Eq. (5) to represent the experimental data to estimate the deposition of ultrafine 3D printing particles in TB airways.

Based on the data acquired from the experiments using NaCl ultrafine particles for wall-loss studies, the wall-loss correction equation was found to be

$$L(R, d) = (1 + 0.01R + 0.02\ R^{0.5})\ (1.5\ d^{-0.9}) \tag{6}$$

where d is the particle diameter (from 10 to 100 nm) and R is the lowest bifurcation generation in the airway replica (from 0 to 11). Therefore, by obtaining Eq. (5) and Eq. (6), the deposition fractions of ultrafine 3D printing particles in a specific bifurcation generation could be estimated based on Eq. (5) + Eq. (6) and Eq. (2).

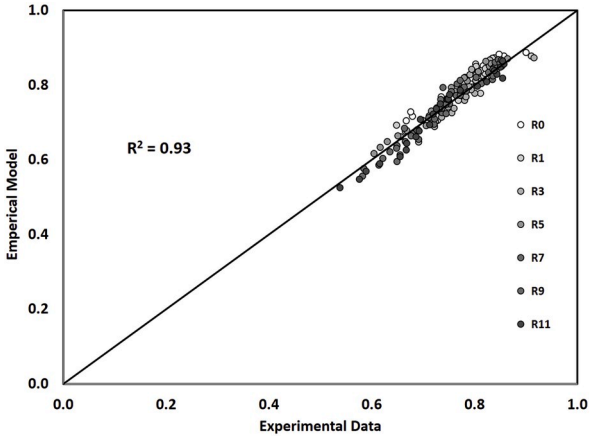

Fig. 7. The coefficient of determination for the experimental data and empirical model data of the outlet-to-inlet concentration ratio (C_{out}/C_{in}) for different R_i.

Fig. 8 presents the estimated cumulative deposition fractions in the TB airways. As expected, the smaller the particle size, the higher the cumulative deposition in the TB airways will be. The deposition increased as the total included bifurcation generations increased. The G1 to G11 cumulative deposition fractions were estimated to be 1%–13% depending on the particle size. Fig. 9 shows the data comparison between the raw experimental data and the corresponding empirical model estimations with and without wall-loss corrections. As can be seen, the estimated result without wall-loss correction was found to agree fairly well with the raw experimental data indicating that the empirical model developed in Eq. (5) worked as expected. The cumulative deposition dropped 5.2% at 10 nm, 2.5% at 30 nm, and 1.1% at 100 nm after wall-loss corrections. These results suggest the inherent wall-loss at corresponding particle sizes in the MALDA under the 30 L/min inspiratory flow rate used.

Fig. 10 presents the comparison between the model-estimated cumulative deposition from G1 to G11 and the ICRP (International Commission on Radiological Protection) conventional deposition curve for the entire TB airways (ICRP, 1994). The difference in the deposition fractions ranged from 12.1% to 1.6% depending on the particle size. Also plotted in Fig. 10 for comparison is the G1 to G11 cumulative deposition estimated by the empirical model associated with NaCl particles (wall-loss correction considered). As can be seen, the estimated cumulative deposition of ultrafine NaCl particles showed higher than that of ultrafine 3D printing particles. This result implies that the ultrafine 3D printing particles generate a slightly lower respiratory deposition in the human TB airways in general. The reason for the low cumulative respiratory deposition shown in Fig. 10 was not clear. A possible explanation might be the complexity of 3D printing emissions, which involves vapor condensation/nucleation, vapor and particle interaction, possible particle agglomeration, and temperature changes. In contrast, in our previous study on ultrafine welding fume particles (Su et al., 2019), the estimated cumulative deposition in the entire TB airways was found to be higher than the NaCl particles.

Nevertheless, results obtained from this study demonstrate that the cumulative deposition of ultrafine 3D printing particles in the TB airways can be efficiently and systematically measured by the newly developed MALDA approach. It is worth noting that, for a set of seven deposition experiments (R0 to R11 in odd numbers) with one run for each *Ri*, the total time needed to complete the measurements was less than 60 min. This prominent time-efficient feature suggests that the MALDA approach can be well suited for future inhalation dosimetry tests. When the airway replicas can be made available for further lower human airways or even the alveolar region by the state-of-the-art, high-resolution 3D printing technology, the function of the MALDA can be greatly enhanced. By then, the MALDA can be a powerful tool for conducting on-site ultrafine particles respiratory deposition experiments to collect *in situ*, real-time data to assist occupational and environmental health associated exposure assessments and risk analyses.

4. Conclusion

In this study, a recently developed and upgraded MALDA was applied to study the respiratory deposition of ultrafine particles emitted from a 3D printer. Data acquired showed new lung deposition data obtained in the human TB airways down to the 11th bifurcation generation. The estimation of the respiratory deposition was facilitated by an empirical model developed based on the experimental data. Deposition results showed that the cumulative depositions of ultrafine 3D printing particles in the TB airways from G1 to G11 were 1%–13%, depending on the particle size. Overall, the newly developed MALDA approach was a useful and efficient tool for characterizing the respiratory deposition of ultrafine particles in the human TB airways.

Funding

Funding for this study was supported by PRIME Grant from the School of Public Health, UTHealth and Grant No. 5T42OH00842109 from the National Institute for Occupational Safety and Health (NIOSH) / Centers for Disease Control and Prevention (CDC) to the Southwest Center for Occupational and Environmental Health (SWCOEH), a NIOSH Education and Research Center.

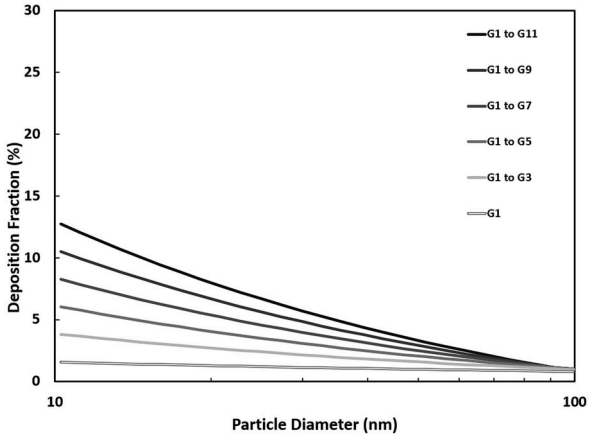

Fig. 8. The estimated cumulative deposition in TB airways for different numbers in bifurcation generations.

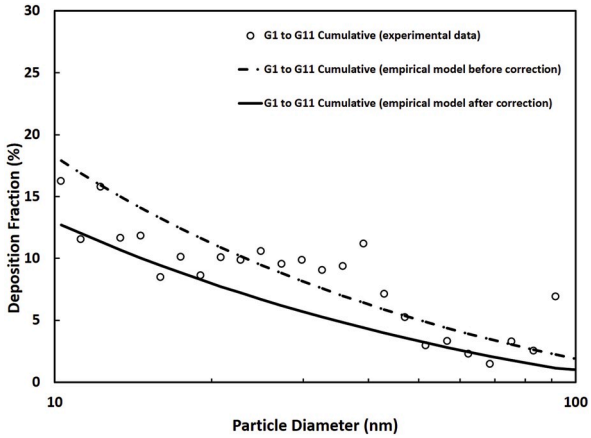

Fig. 9. The comparison of the cumulative deposition between experimental data and model data before and after wall-loss correction.

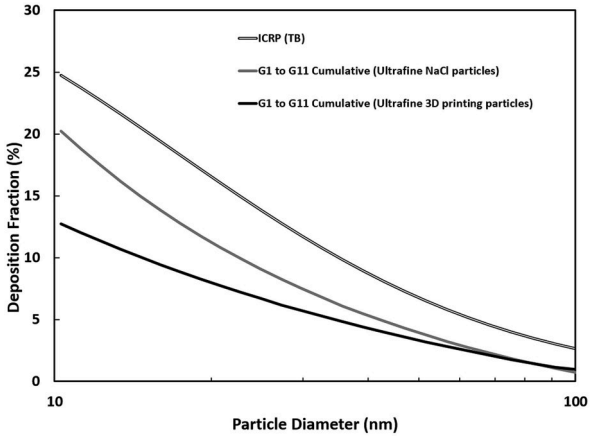

Fig. 10. The comparison of the estimated cumulative deposition in the TB airways.

References

Azimi, P., Zhao, D., Pouzet, C., Crain, N. E., & Stephens, B. (2016). Emissions of ultrafine particles and volatile organic compounds from commercially available desktop three-dimensional printers with multiple filaments. *Environmental Science & Technology, 50*(3), 1260–1268.

Campbell, T., Williams, C., Ivanova, O., & Garrett, B. (2011). *Could 3D printing change the world? Technologies, potential, and Implications of additive manufacturing, A strategic foresight report*. Washington DC: Atlantic Council.
Chan, F., Rajaram, N., House, R., Kudla, I., Lipszyc, J., & Tarlo, S. M. (2017). Potential respiratory effects from 3-D printing. In *B58. Occupational lung Disease: Case studies, epidemiology, and mechanisms*. American Thoracic Society. A3861-A3861.
Cheng, Y. S., Zhou, Y., & Chen, B. T. (1999). Particle deposition in a cast of human oral airways. *Aerosol Science & Technology, 31*(4), 286–300.
Deng, Y., Cao, S. J., Chen, A., & Guo, Y. (2016). The impact of manufacturing parameters on submicron particle emissions from a desktop 3D printer in the perspective of emission reduction. *Building and Environment, 104*, 311–319.
Gu, J., Wensing, M., Uhde, E., & Salthammer, T. (2019). Characterization of particulate and gaseous pollutants emitted during operation of a desktop 3D printer. *Environment International, 123*, 476–485.
He, W., Zhao, Y. B., Jiang, F., Guo, Y., Gao, H., Liu, J., & Wang, J. (2020). Filtration performance and charge degradation during particle loading and reusability of charged PTFE needle felt filters. *Separation and Purification Technology, 233*, 116003.
Hinds, W. C. (1999). *Aerosol technology: Properties, behavior, and measurement of airborne particles. Appendix A 11*. New York, NY: John Wiley & Sons.
House, R., Rajaram, N., & Tarlo, S. M. (2017). Case report of asthma associated with 3D printing. *Occupational Medicine, 67*(8), 652–654.
ICRP. (1994). *Human respiratory tract model for radiological protection. Publication 66, Ann. ICRP 24* (pp. 1–3). Oxford: Pergamon Press.
Kitaoka, H., Koc, S., Tetsumoto, S., Koumo, S., Hirata, H., & Kijima, T. (2013). 4D model generator of the human lung, "Lung4Cer". In *Conf proc IEEE eng med biol soc 2013* (pp. 453–456).
Kitaoka, H., Takaki, R., & Suki, B. (1999). A three-dimensional model of the human airway tree. *Journal of Applied Physiology, 87*(6), 2207–2217.
Kreyling, W. G., Semmler-Behnke, M., & Möller, W. (2006). Ultrafine particle–lung interactions: Does size matter? *Journal of Aerosol Medicine, 19*(1), 74–83.
Lipson, H., & Kurman, M. (2013). *Fabricated: The new world of 3D printing*. New York, NY: John Wiley & Sons.
Miller, F. J., Asgharian, B., Schroeter, J. D., & Price, O. T. (2016). Improvements and additions to the multiple path particle dosimetry model. *Journal of Aerosol Science, 99*, 14–26.
Oberdörster, G. (2001). Pulmonary effects of inhaled ultrafine particles. *International Archives of Occupational and Environmental Health, 74*(1), 1–8.
Phalen, R. F., Oldham, M. J., Mannix, R. C., & Schum, G. M. (1997). Deposition of fluorescent particles in replica casts of distal human airways: Comparison of theory with experiment. *Annals of Occupational Hygiene, 41*, 565–570. inhaled_particles_VIII.
Potter, P. M., Al-Abed, S. R., Lay, D., & Lomnicki, S. M. (2019). VOC emissions and formation mechanisms from carbon nanotube composites during 3D printing. *Environmental Science & Technology, 53*(8), 4364–4370.
Ryi, S. K., Park, J. S., Park, S. J., Lee, D. G., & Kim, S. H. (2007). Fabrication of nickel filter made by uniaxial pressing process for gas purification: Fabrication pressure effect. *Journal of Membrane Science, 299*(1-2), 174–180.
Smith, S., Cheng, Y. S., & Yeh, H. C. (2001). Deposition of ultrafine particles in human tracheobronchial airways of adults and children. *Aerosol Science & Technology, 35*(3), 697–709.
Stabile, L., Scungio, M., Buonanno, G., Arpino, F., & Ficco, G. (2017). Airborne particle emission of a commercial 3D printer: The effect of filament material and printing temperature. *Indoor Air, 27*(2), 398–408.
Stephens, B., Azimi, P., El Orch, Z., & Ramos, T. (2013). Ultrafine particle emissions from desktop 3D printers. *Atmospheric Environment, 79*, 334–339.
Su, W. C., Chen, Y., Bezerra, M., & Wang, J. (2019b). Respiratory deposition of ultrafine welding fume particles. *Journal of Occupational and Environmental Hygiene, 16*(10), 694–706.
Su, W. C., & Cheng, Y. S. (2009). Deposition of man-made fibers in human respiratory airway casts. *Journal of Aerosol Science, 40*(3), 270–284.
Su, W. C., Chen, Y., & Xi, J. (2019a). A new approach to estimate ultrafine particle respiratory deposition. *Inhalation Toxicology, 31*(1), 35–43.
Su, W. C., Ku, B. K., Kulkarni, P., & Cheng, Y. S. (2016). Deposition of graphene nanomaterial aerosols in human upper airways. *Journal of Occupational and Environmental Hygiene, 13*(1), 48–59.
Vance, M. E., Pegues, V., Van Montfrans, S., Leng, W., & Marr, L. C. (2017). Aerosol emissions from fuse-deposition modeling 3D printers in a chamber and in real indoor environments. *Environmental Science & Technology, 51*(17), 9516–9523.
Wojtyła, S., Klama, P., & Baran, T. (2017). Is 3D printing safe? Analysis of the thermal treatment of thermoplastics: ABS, PLA, PET, and nylon. *Journal of Occupational and Environmental Hygiene, 14*(6), D80–D85.
Zhang, Q., Wong, J. P., Davis, A. Y., Black, M. S., & Weber, R. J. (2017). Characterization of particle emissions from consumer fused deposition modeling 3D printers. *Aerosol Science and Technology, 51*(11), 1275–1286.
Zhou, Y., & Cheng, Y. S. (2005). Particle deposition in a cast of human tracheobronchial airways. *Aerosol Science and Technology, 39*(6), 492–500.
Zukas, V., & Zukas, J. A. (2015). *An introduction to 3D printing*. Sarasota, FL: First Edition Design Publisher.